Dune formation on the present Mars

Eric J. R. Parteli[1,2] and Hans J. Herrmann[2,3]
[1]*Institut für Computerphysik, ICP, Universität Stuttgart, Pfaffenwaldring 27, 70569 Stuttgart, Germany*
[2]*Departamento de Física, Universidade Federal do Ceará-60455-760, Fortaleza, CE, Brazil*
[3]*Computational Physics, IfB, ETH Hönggerberg, HIF E 12, CH-8093, Zürich, Switzerland*
(Received 1 May 2007; revised manuscript received 9 August 2007; published 31 October 2007)

We apply a model for sand dunes to calculate formation of dunes on Mars under the present Martian atmospheric conditions. We find that different dune shapes as those imaged by Mars Global Surveyor could have been formed by the action of sand-moving winds occuring on today's Mars. Our calculations show, however, that Martian dunes could be only formed due to the higher efficiency of Martian winds in carrying grains into saltation. The model equations are solved to study saltation transport under different atmospheric conditions valid for Mars. We obtain an estimate for the wind speed and migration velocity of barchan dunes at different places on Mars. From comparison with the shape of bimodal sand dunes, we find an estimate for the time scale of the changes in Martian wind regimes.

DOI: 10.1103/PhysRevE.76.041307 PACS number(s): 45.70.−n, 45.70.Qj, 92.60.Gn, 96.30.Gc

I. INTRODUCTION

Sand dunes are ubiquitous on Mars and provide evidence that sand-moving winds have once occured on the red planet. However, Martian dunes do not appear to be moving these days, and thus many authors suggested that dunes on Mars have been formed in the past, when the climate of Mars was much more Earthlike [1]. On a planet where the present atmospheric density is almost 100 times lower than the Earth's, only winds one order of magnitude stronger than on Earth are able to transport sand and form dunes [2,3]. Such strong winds occur in fact only occasionaly on Mars, during the strongest dust storms [4,5]. Only once during the Viking mission, which operated for about 6 terrestrial years, could very little changes on Martian soils be detected after such a storm [6]. Moreover, calculations showed that the sand-moving winds that occurred at the Viking landing site lasted for not more than a few tens of seconds [4,6]. Could Martian dunes have been formed by the action of such rarely occuring winds under the atmosphere of the present Mars? This is the question that motivates the present work.

The sand that forms dunes is transported by the wind through *saltation*, which consists of grains traveling in a sequence of ballistic trajectories and producing a *splash* of new ejected grains when impacting onto the ground [7]. Martian saltation has been studied in wind tunnel experiments and also in numerical simulations [8,9]. Due to the thinner atmosphere of Mars and owing to the lower gravity $g=3.71\ \mathrm{m/s^2}$, which is nearly 1/3 of the Earth's gravity, saltating grains on Mars travel longer and higher than their terrestrial counterparts [9]. Moreover, Martian grains also saltate with faster velocities than grains on our planet. As consequence, the grain-bed collisions or *splash* events on Mars are expected to be much larger than on Earth, due to the larger momentum transferred by the impacting grains to the sand bed [10].

What is not known is whether such highly energetic saltation events have been responsible for the formation of the enormous dunes observed in the images of Mars. In order to understand this, it is necessary to investigate sand transport at length scales comparable to the scale of dunes. Once saltation starts, the wind transfers momentum to accelerate the grains. Thus the momentum of the air decreases as the flux of saltating particles increases ("feedback effect" [11]). After a distance which is called "saturation length," the wind strength is just sufficient to sustain saltation, and the sand flux achieves saturation. In this manner, dunes that have length smaller than the saturation length will be continuously eroded due to increase of the sand flux and will disappear. In other words, the existence of a minimal dune size is related to the phenomenon of flux saturation, which could not be investigated from wind tunnel simulations of Martian saltation [9,10]. While the first wind tunnel simulating Martian conditions is a few meters long, the smallest dunes on Mars have length of the order of 100 m (Fig. 1).

Recently, a successful modeling of the formation of sand dunes, which encompasses the main processes of saltation and accounts for flux saturation and the existence of a minimal dune size, has been achieved [12,13]. This model consists of a system of continuum equations in two space dimensions which reproduce the shape of terrestrial dunes, the wind profile and the sand flux, and provide excellent quantitative agreement with measurements [14]. The dune model, which has been applied to study the interaction of dunes in a field [15] and the formation of parabolic dunes in the presence of vegetation [16], has become a powerful tool in the investigation of the large time-scale processes involved in the formation of desert and coastal landscapes.

In the present work, which is the extended version of a recent paper [17], we apply the dune model to investigate whether dunes could be formed on the present Mars. Our aim is to reproduce the shape of Martian dunes using the present Martian atmospheric conditions. The dune model has parameters of atmosphere, wind and sand, many of which are known for Mars and can be therefore used to solve the model equations. While most of the quantities controlling saltation can be calculated from the atmospheric density ρ_{fluid}, gravity g, air viscosity η, and from the grain diameter d, there is one unknown quantity, which is related to the intensity of the Martian splash and must be determined from simulations. Moreover, the wind velocity that formed Martian dunes is

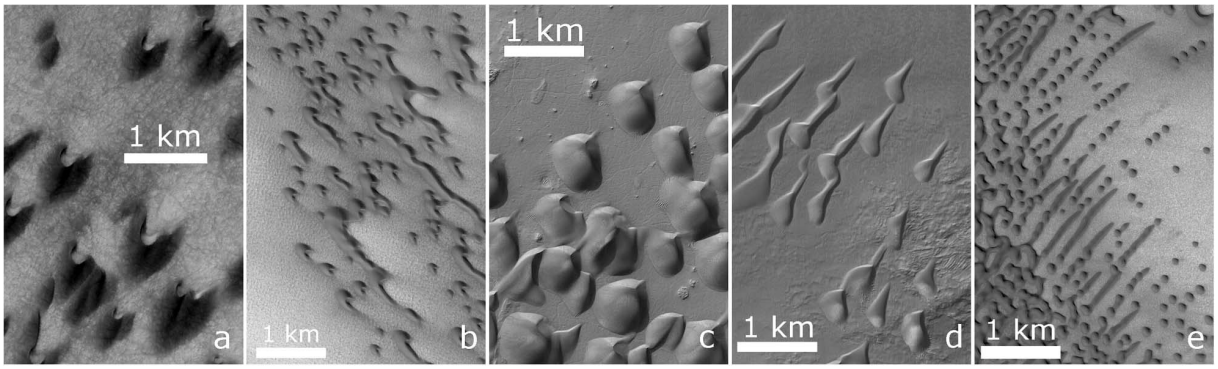

FIG. 1. Mars Global Surveyor (MGS), Mars Orbiter Camera (MOC) images of sand dunes on Mars (courtesy of NASA/JPL/MSSS). From the left to the right: (a) Barchan dunes at Arkhangelsky crater, near 41.0°S, 25.0°W; (b) north polar dunes near 77.6°N, 103.6°W; bimodal sand dunes near (c) 48.6°S, 25.5°W; (d) 49.6°S, 352.9°W, and (e) 76.4°N, 272.9°W.

also a parameter: it must be estimated from comparison with the shape of the dunes.

This paper is organized as follows. In the next section we describe the dune model. In Sec. III we calculate the average grain velocities, mean saltation height, and sand flux on Mars from the known parameters, and the results are compared with wind tunnel predictions and with calculation results for saltation transport on Earth. In Sec. IV we present in detail the calculations of Mars dunes that have been published in the preceding paper [17]. We begin with the simplest dune form, which is the barchan dune. First, we study the shape of the barchan dunes in the Arkhangelsky crater. We find an equation for the rate at which grains enter saltation, which can be used in the calculations of dunes under different atmospheric conditions. We then estimate the wind velocity on Mars and predict the migration velocity of Martian barchans. Next, we study the shape of Martian bimodal sand dunes and find an estimate for the time scale of changes in wind regimes on Mars. Conclusions are presented in Sec. V.

II. DUNE MODEL

The dune model combines an analytical description of the average turbulent wind velocity field above the dune with a continuum saltation model which allows for saturation transients in the sand flux. Here we give a brief presentation of the model and refer to Sauermann *et al.* [13], Schwämmle and Herrmann [18], and Durán and Herrmann [19] for the extensive derivation of the saltation transport equations.

A. Wind

In the turbulent boundary layer, where sand transport takes place, the velocity of the wind $u(z)$ increases logarithmically with height z above the flat ground:

$$u(z) = \frac{u_*}{\kappa} \ln \frac{z}{z_0}, \tag{1}$$

where $\kappa = 0.4$ is the von Kármán constant, u_* is the wind shear velocity, which is used to define the shear stress $\tau = \rho_{\text{fluid}} u_*^2$, and z_0 is the aerodynamic roughness. u_* and z_0 can be determined from measurements of the wind velocity at different heights, as done for instance in the Mars Pathfinder Lander Wind Sock Experiment [20]. The aerodynamic roughness z_0 is larger than the surface roughness of the undisturbed sand bed, z_0^{sand}, which is of the order of a few tens of microns and is due to the microscopic fluctuations of the sand bed when the grains are at rest [7]. A value of z_0 close to 1.0 mm has been often reported from measurements of terrestrial saltation on a sand bed [21], while on Mars z_0 is larger, around 1.0 cm [20].

In fact, many studies showed that the effective aerodynamic roughness z_0 depends on the friction velocity u_* (e.g., Refs. [7,11,22]). However, since the study of the present work is limited to a narrow range of friction velocity (between u_{*t} and $2u_{*t}$), the aerodynamic roughness can be considered as constant. It is interesting [23] that using the formula $z_0 = 0.04 u_*^2/2g$ proposed by Owen [11], with $u_* = 2.0$ m/s and $g = 3.71$ m/s^2, we obtain $z_0 \simeq 2.0$ cm, which is not far from the value obtained in Ref. [20].

A dune or a smooth hill introduces a perturbation in the shear stress whose Fourier-transformed components are calculated using the algorithm of Weng *et al.* [24]:

$$\tilde{\hat{\tau}}_x = \frac{2h(k_x,k_y)k_x^2}{|k|U^2(l)}\left[1 + \frac{2\ln(\mathcal{L}|k_x|) + 4\epsilon + 1 + i\,\text{sign}(k_x)\pi}{\ln(l/z_0)}\right] \tag{2}$$

and

$$\tilde{\hat{\tau}}_y = \frac{2h(k_x,k_y)k_x k_y}{|k|U^2(l)}, \tag{3}$$

where the coordinate axes x and y are parallel, respectively, perpendicular to the wind direction, k_x and k_y are wave numbers, $|k| = \sqrt{k_x^2 + k_y^2}$, and $\epsilon = 0.577\,216$ (Euler's constant). $\mathcal{L}$ is the horizontal distance between the position of maximum height, $H_{\max}$, and the position of the windward side where the height is $H_{\max}/2$ [24]. $U(l) = u(l)/u(h_m)$ is the undisturbed wind velocity at height $l = 2\kappa^2\mathcal{L}/\ln l/z_0$ normalized by the velocity at the reference height $h_m = \mathcal{L}/\sqrt{\log \mathcal{L}/z_0}$, which separates the middle and upper flow layers [24]. The shear stress in the direction i $(i = x, y)$ is then given by $\vec{\tau}_i = \hat{i}[\tau_0(1$

$+\hat{\tau}_i)]$, where τ_0 is the undisturbed shear stress over the flat ground.

Sand transport occurs if u_* exceeds a threshold velocity for entrainment, $u_{*\mathrm{ft}}$, which depends on d, g, ρ_{fluid}, on the grain density ρ_{grain}, and also on the internal friction of the granular material [25]. Indeed, the wind velocity may even decrease to values lower than $u_{*\mathrm{ft}}$, and still saltation can be sustained, once initiated. This is because the splash is the most important mechanism of sand entrainment during saltation [7]. The wind strength, however, cannot be lower than the impact threshold velocity $u_{*\mathrm{t}}$, which defines the threshold shear stress $\tau_{\mathrm{t}}=\rho_{\mathrm{fluid}}u_{*\mathrm{t}}^2$ and is around 80% of $u_{*\mathrm{ft}}$. Saltation ceases if $u_*<u_{*\mathrm{t}}$, and therefore the impact threshold velocity is the essential threshold velocity for aeolian sand transport.

B. Continuum saltation model

The wind shear velocity computed above is used to calculate the sand flux with the model derived in Sauermann *et al.* [13]. The sand bed represents an open system which can exchange grains with the moving saltation layer, for which the erosion rate $\Gamma(x,y)$ at any position (x,y) represents a source term. Mass conservation yields that the local change in the flux balances the erosion rate:

$$\vec{\nabla}\cdot(\rho\vec{v})=\Gamma(x,y), \tag{4}$$

where $\rho(x,y)$, which has unit of mass per unit surface, is the surface density of the saltation layer, i.e., the volume density integrated over the saltation layer depth, and $\vec{v}(x,y)$ is the average local velocity of the saltating grains [13].

The erosion rate is the difference between the vertical flux of ejected grains and the vertical flux ϕ of grains impacting onto the bed:

$$\Gamma=\phi(n-1), \tag{5}$$

where $\phi=\rho|\vec{v}|/\ell$, ℓ is the average saltation length (Appendix A), and n is the average number of splashed grains. At saturation, the air shear stress τ_{a} decreases to the threshold τ_{t}, and the following expression is obtained for n [13]:

$$n=1+\tilde{\gamma}\left(\frac{\tau_{\mathrm{a}}}{\tau_{\mathrm{t}}}-1\right), \tag{6}$$

where $\tilde{\gamma}=dn/d(\tau_{\mathrm{a}}/\tau_{\mathrm{t}})$, the *entrainment rate* of grains into saltation, determines how fast the system reaches saturation [13].

Thus inserting Eq. (6) into Eq. (5), and substituting this into Eq. (4), we obtain a differential equation for the sand flux. However, in the model, the average grain velocity is calculated in the *steady state*, i.e., $\vec{v}=\vec{v}_{\mathrm{s}}$, using the value of reduced wind velocity at a reference height z_1 between the roughness height and the mean saltation height z_{m} [13]. The equations used in the calculation of $\vec{v}_{\mathrm{s}}$ are displayed in Appendix B, and we refer to Sauermann *et al.* [13] for their detailed derivation.

In this manner, the mass conservation equation can be written in terms of the *sand flux*,

$$\vec{q}=\rho\vec{v}_{\mathrm{s}}, \tag{7}$$

and the *saturated sand* flux,

$$q_{\mathrm{s}}=\frac{2\alpha|\vec{v}_{\mathrm{s}}|}{g}(\tau-\tau_{\mathrm{t}})=\frac{2\alpha|\vec{v}_{\mathrm{s}}|}{g}u_{*\mathrm{t}}^2[(u_*/u_{*\mathrm{t}})^2-1]. \tag{8}$$

The resulting equation for the sand flux is a differential equation that contains the saturated flux q_{s} at the steady state,

$$\vec{\nabla}\cdot\vec{q}=\frac{1}{\ell_{\mathrm{s}}}|\vec{q}|\left(1-\frac{|\vec{q}|}{q_{\mathrm{s}}}\right), \tag{9}$$

where the *saturation length*, ℓ_{s}, contains the information of the saturation transient of the sand flux. ℓ_{s} is written as

$$\ell_{\mathrm{s}}=\frac{1}{\tilde{\gamma}}\left[\frac{\ell}{(u_*/u_{*\mathrm{t}})^2-1}\right]=\frac{1}{\gamma}\left[\frac{2|\vec{v}_{\mathrm{s}}|^2\alpha/g}{(u_*/u_{*\mathrm{t}})^2-1}\right], \tag{10}$$

where we defined

$$\gamma=r\tilde{\gamma}=\frac{|\vec{v}_{\mathrm{s}}|}{\Delta v_{\mathrm{hor}}}\left[\frac{dn}{d(\tau_{\mathrm{a}}/\tau_{\mathrm{t}})}\right], \tag{11}$$

in which $r\equiv|\vec{v}_{\mathrm{s}}|/\Delta v_{\mathrm{hor}}$. The quantity γ incorporates, thus, the entrainment rate $\tilde{\gamma}=dn/d(\tau_{\mathrm{a}}/\tau_{\mathrm{t}})$, which gives the amount n of grains launched when the air shear stress τ_{a} deviates from the threshold by an amount $\tau_{\mathrm{a}}-\tau_{\mathrm{t}}$. γ contains therefore the information of the intensity of the splash.

C. Surface evolution

The change in the surface is computed using the flux calculated with Eq. (9). The time evolution of the topography $h(x,y,t)$ is given by the mass conservation equation:

$$\frac{\partial h}{\partial t}=-\frac{1}{\rho_{\mathrm{sand}}}\vec{\nabla}\cdot\vec{q}, \tag{12}$$

where $\rho_{\mathrm{sand}}=0.62\rho_{\mathrm{grain}}$ is the mean density of the immobile sand which constitutes the sand bed [13].

The dune model can be sketched as follows.

(1) The shear stress over the surface is calculated with the algorithm of Weng *et al.* [24], using Eqs. (2) and (3).

(2) From the shear stress, the sand flux is calculated using Eq. (9), where the saturation length ℓ_{s} and the saturated sand flux q_{s} are calculated from expressions (10) and (8), respectively.

(3) The change in the surface height is computed from mass conservation [Eq. (12)] using the calculated sand flux.

(4) Avalanches occur wherever the inclination exceeds the angle of repose $\theta_{\mathrm{r}}=34°$, then the slip face is formed. At the dune brink, flow separation occurs. In the model, the dune is divided into several two-dimensional (2D) slices parallel to wind direction, and for each slice, one separation streamline is introduced at the lee side as described in detail in Ref. [12]. Each streamline is fitted by a third order polynomial connecting the brink with the ground at the reattachment point [12], and defining the "separation bubble," in which the wind and the flux are set to zero.

Calculations are performed using open boundaries with a constant influx of sand, q_{in}, at the inlet. The influx is interpreted as the average flux between the dunes, which is typically between 10% and 40% of the maximum flux q_{s} [26],

and is considered, for simplicity, homogeneous along the y axis (perpendicular to sand transport). The model is evaluated by performing steps (1)–(4) computationally in a cyclic manner.

Model parameters. With the equations presented in Appendix C, the model parameters can be calculated from the following quantities: ρ_{fluid}, g, d, ρ_{grain}, and from the viscosity η. Thus these quantities are, together with γ [Eq. (11)] and with the shear velocity u_*, the only parameters of the model. The threshold velocity $u_{*\text{t}}$ is obtained with Eq. (C1), the drag coefficient C_{d} is given by Eq. (C4), while Eqs. (C8)–(C11) are used to obtain z_1, z_{m}, z_0^{sand}, and α.

III. SALTATION TRANSPORT ON MARS

Since the quantities governing saltation are functions of the atmospheric conditions, we expect saltation to be different depending on the location on Mars. The reason is that the average atmospheric pressure and temperature may vary within an extremely wide range compared to the terrestrial case. In this section, we estimate the average trajectories of saltating grains and the sand flux under different atmospheric conditions on Mars. The results presented in this section are then used in the next sections to calculate formation of dunes on Mars.

A. Martian atmosphere

The Mars Global Surveyor Radio Science (MGSRS) Team has provided valuable atmospheric data of Mars [27]. In particular, the temperature T and the pressure P near the surface have been systematically measured in many locations of Mars. We use the ideal gas equation to calculate the local atmospheric density, ρ_{fluid}, from the MGSRS pressure and temperature data. An atmosphere of 100% CO_2 is considered. Furthermore, the dynamic viscosity η of the Martian atmosphere is a function of the temperature T, and is calculated using the Sutherland's formula [28]:

$$\eta = \eta_0 \left[\frac{T_0 + C}{T + C} \right] (T/T_0)^{3/2}, \tag{13}$$

where for CO_2 we have $\eta_0 = 1.48 \times 10^{-5}$ kg/m s, $C=240$, and $T_0 = 293.15$ K [28]. Finally, the kinematic viscosity ν is calculated with the equation $\nu = \eta/\rho_{\text{fluid}}$.

B. Particle size of Martian dunes

Edgett and Christensen [29] have used thermal inertia data to obtain the grain diameter of dunes in intracrater fields of dark dunes on Mars. They found that the average grain diameter of Martian dunes is $d = 500 \pm 100$ μm, which is coarser than the mean diameter of terrestrial dune grains, 250 μm [21]. The value of mean grain diameter $d = 500$ μm as measured by Edgett and Christensen [29] for dunes on Mars is used in the calculations of the present work, while $d = 250$ μm is considered for terrestrial dunes. Furthermore, we take the density $\rho_{\text{grain}} = 3200$ and 2650 kg/m^3 for Martian [30] and terrestrial [7] grains, respectively.

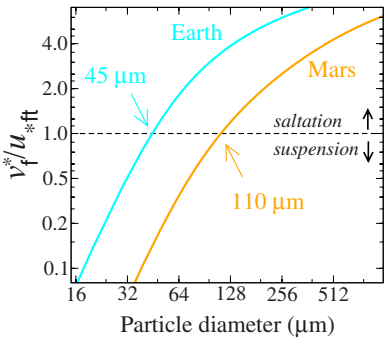

FIG. 2. (Color online) Ratio between the relative grain velocity v_{f}^* and the threshold friction speed for saltation, $u_{*\text{ft}}$, calculated for Mars and for Earth as a function of the grain diameter d. The dashed line indicates the saltation-suspension transition at $v_{\text{f}}^*/u_{*\text{ft}} = 1.0$, and intercepts the Martian (terrestrial) continuous line at $d = 110$ μm ($d = 45$ μm).

Why is the sand of Martian dunes coarser than the sand of Earth's dunes? There is a critical value of the diameter d, below which the particle remains suspended in the atmosphere. The critical diameter depends on the vertical fluctuating component of the wind velocity u' [31]. It has been suggested that if the standard deviation of u', which scales with the wind friction speed, is larger than the settling velocity of the grain, v_{f}, then the particle will remain suspended [29,31]. The falling velocity v_{f} is obtained from the equilibrium between the gravitational force and the fluid drag [32]. Particles for which the ratio $v_{\text{f}}/u_{*\text{ft}}$ is smaller than 1.0 enter suspension [31]. In this manner, a critical grain diameter of 210 μm is obtained for Mars, while on Earth the critical value is about 52 μm [29].

The critical diameter obtained in this manner for Mars appears inconsistent with the observation of Martian aeolian ripples composed of grains of diameter around 100 μm [5,33]. Here we calculate the transition suspension-saltation using the relative velocity $v_{\text{f}}^* = v_{\text{f}}/\sqrt{2\alpha}$ [Eq. (B4)] obtained from the equilibrium between the fluid drag and the bed friction τ_{g}. This velocity includes the information of the *shape* of the average saltation trajectories in the equilibrium, since the effective restitution coefficient of the splash, $\alpha = v_z^{\text{eje}}/\Delta v_{\text{hor}}$, determines the vertical velocity of ejection, v_z^{eje}, in response to the horizontal velocity gain of the saltating grains, Δv_{hor} [13]. Δv_{hor} is proportional to the average grain velocity v_{s}, which enters the expression of the mean saltation length ℓ (Appendix A). Moreover, the value of the drag coefficient C_{d} considered for particles in the saltation cloud differs from the drag coefficient for a vertically falling grain since in Eq. (C4) the parameter α also appears. This is because in the equilibrium, the mean drag on the saltating grains compensates the average loss of momentum due to the grain-bed collisions, or bed friction, the expression for which incorporates the quantity α [13,19].

Figure 2 shows the ratio $v_{\text{f}}^*/u_{*\text{ft}}$ as a function of the grain diameter d, calculated using parameters for Earth and for Mars, where we used the nominal pressure $P = 6.0$ mbar and temperature $T = 200$ K for Mars. In this figure, the threshold shear velocity for saltation, $u_{*\text{ft}} = 1.25 u_{*\text{t}}$, is calculated using Eq. (C1), while v_{f}^* is calculated with Eq. (B4). The dashed

TABLE I. Main quantities controlling saltation on Mars under several values of pressure P and temperature T, and a *constant* $u_*/u_{*t}=1.5$. The threshold shear velocity u_{*t}, the mean saltation height z_m, the drag coefficient C_d, and the model variables z_1 and α depend on the atmospheric conditions and have been calculated for a constant grain diameter $d=500$ μm and density $\rho_{grain}=3200$ kg/m^3, and with a dynamic viscosity obtained from the temperature (Eq. (13)). The grain velocity v_s and the saturated flux q_s have been calculated with Eqs. (B3) and (8), respectively. The corresponding values for terrestrial saltation are shown in the last line of the table for comparison. On Earth, the value $u_*=1.5u_{*t}$ means a shear velocity of 0.32 m/s.

P (mbar)	T (K)	u_{*t} (m/s)	z_m (m)	z_1 (m)	α	C_d	v_s (m/s)	q_s (kg/m s)
5.0	150	1.804	0.789	0.011	0.300	3.744	13.132	0.152
5.0	200	2.162	1.154	0.014	0.227	5.043	18.017	0.170
5.0	250	2.487	1.543	0.017	0.184	6.505	22.957	0.187
7.5	150	1.449	0.553	0.009	0.339	3.331	9.964	0.127
7.5	200	1.736	0.810	0.012	0.257	4.389	13.617	0.141
7.5	250	1.996	1.082	0.015	0.209	5.567	17.338	0.154
10.0	150	1.241	0.431	0.008	0.371	3.083	8.205	0.111
10.0	200	1.486	0.630	0.011	0.280	4.001	11.173	0.123
10.0	250	1.708	0.841	0.014	0.228	5.015	14.210	0.135
1000	300	0.218	0.016	0.004	0.431	2.747	1.419	0.009

line indicates the transition value $v_f^*/u_{*ft}=1.0$.

As we can see from Fig. 2, particles with a diameter smaller than 45 μm enter suspension on Earth, while the critical value of d on Mars is around 110 μm. The value of the critical diameter on Earth obtained in Fig. 2 is similar to the one predicted from v_f/u_{*ft} because 2α on Earth is close to unity (Table I). However, the Martian value of critical grain diameter is much smaller than the one obtained in previous calculations [29]. As shown in Table I, values of α on Mars are lower than on Earth, which means much flatter saltation trajectories on Mars, as observed in wind tunnel experiments [9], due to the smaller Martian average ejection angles. In this manner, Fig. 2 suggests that the previously reported inadequacy of v_f/u_{*ft} to characterize the transition suspension-saltation on Mars [5] arises from the lower aspect ratio (height/length) of the average grain trajectories on Mars, which allows grains of size smaller than the one predicted with v_f/u_{*ft} to remain in saltation.

Furthermore, we see that the ratio between the measured average grain size of dunes (500 and 250 μm on Mars and on Earth, respectively) and the critical diameter obtained in Fig. 2 is around 5.0 on both planets. In fact, pure saltation is expected to occur only if the falling velocity is larger than 2.5 u_{*t}, which explains why the sand of dunes is effectively much larger than the critical diameter [29].

C. Saltation trajectories and sand flux

The model parameters that govern the grain trajectories are the average saltation height, z_m [Eq. (C9)]; the reference height z_1 [Eq. (C8)] at which the effective wind velocity u_{eff} is calculated; the drag coefficient, C_d [Eq. (C4)]; and the effective restitution coefficient, α [Eq. (C11)]. From $d=500$ μm, we obtain the surface roughness $z_0^{sand}=25$ μm [Eq. (C10)]. The saturated sand flux q_s [Eq. (8)] is a function of the wind shear velocity u_* and further depends on the saturation velocity of the saltating grains, $v_s=|\vec{v}_s|$, which is calculated in Eq. (B2). The quantities controlling saltation on Mars are calculated in Table I.

In Table I, the model parameters have been calculated using different values of pressure P and temperature T valid for Mars. We see that the minimal friction speed for saltation, u_{*t}, on Mars may vary by a factor of 2. We note that ranges of P and T even wider than the ones studied here may occur on Mars [27]. Moreover, we calculate v_s and q_s in Table I using a constant value of $u_*/u_{*t}=1.5$, since this is a representative value for saltation on Earth [34]. The corresponding values calculated for Earth are shown in the last row of Table I, where we used $d=250$ μm, density $\rho_{fluid}=1.225$ kg/m^3, and viscosity $\eta=1.8$ kg/m s, while $g=9.81$ m/s^2.

We see in Table I that the values of sand flux on Mars are typically ten times larger than on Earth. This is in agreement with the findings from wind tunnel simulations of saltation in a Martian environment by White [9]. We also see that Martian particles travel with higher average velocities, while the mean saltation height z_m on Mars is larger than on Earth, and may be over 1.0 m depending on the atmospheric conditions.

While the ratio u_*/u_{*t} in Table I is constant, in the upper inset of Fig. 3 we calculate q_s for a *constant* wind velocity $u_*=3.0$ m/s using values of P and T within the range studied in Table I. We see that the same wind friction speed transports more sand where P is higher and T is lower, which means lower ρ_{fluid} and u_{*t}.

In the main plot and the lower inset of Fig. 3 we show how the flux and the particle velocity at a given location on Mars depend on u_*/u_{*t}. In the main plot we fix $T=200$ K and calculate the saturated flux q_s for different values of atmospheric pressure P as a function of $u_*/u_{*t}-1$. In the lower inset, the same calculations are made for the grain velocity v_s. We see that the grain velocity in equilibrium is determined by the atmospheric conditions and has only a weak dependence on the friction speed u_*. The equilibrium velocity of the grains, v_s, in fact scales with u_{*t}. Because u_{eff} [Eq.

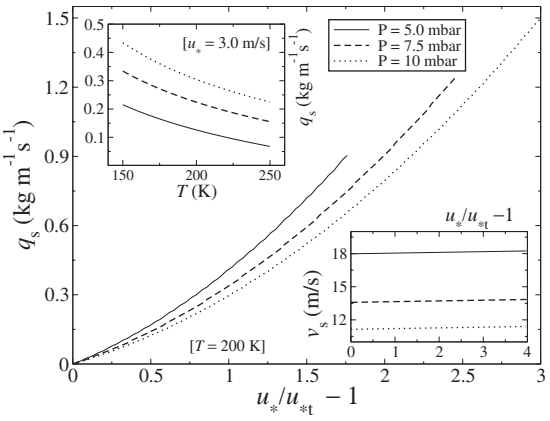

FIG. 3. Main plot: Saturated sand flux q_s as a function of the relative shear velocity $u_*/u_{*t}-1$ for different values of atmospheric pressure—and therefore different values of u_{*t}—obtained with a temperature $T=200$ K. The lower inset on the right shows the corresponding values of the average grain velocity v_s. In the upper inset on the left, we show the saturated flux for $u_*=3.0$ m/s calculated for different values of temperature valid on Mars.

(B1)] and v_f^* [Eq. (B4)] both scale with u_{*t}, v_s also does.

In Fig. 3 we see that for a given value of u_*/u_{*t}, both the flux and the grain velocity are larger for lower atmospheric pressure P. This is because the shear velocity u_{*t} required for sand transport is higher for lower P, while v_s scales with u_{*t} and q_s scales with u_{*t}^2 [Eq. (8)].

Table II shows v_s and q_s calculated for different values of u_*/u_{*t} on Mars and on Earth. Because the threshold wind friction speed on Mars is ten times higher than on Earth, the average velocity of saltating grains on Mars is one order of magnitude higher than the velocity of Earth's grains. Again, v_s may have different values depending on the location on Mars, while q_s depends further on u_*.

In summary, using the atmospheric data provided by the MGS Radio Science Team, we can calculate the quantities controlling saltation at a given location on Mars, for example, at a given dune field. From the "weather" maps [27], we obtain the value of P and T characteristic of the area at which the dune field is located. Next, the density and viscosity are calculated from P and T, using the ideal gas law and Eq. (13), while the model parameters are obtained, as exemplified in Table I, using the grain diameter $d=500$ μm of Martian sand dunes.

TABLE II. Average velocity v_s of saltating grains on Earth and on Mars as a function of the relative shear velocity u_*/u_{*t}. Temperature $T=200$ K and pressure $P=6.0$ mbar were used for Mars.

u_*/u_{*t}	v_s (m/s) [Earth]	v_s (m/s) [Mars]	q_s (kg/m s) [Earth]	q_s (kg/m s) [Mars]
1.05	1.367	15.854	0.0007	0.0128
1.10	1.373	15.857	0.0015	0.0262
1.25	1.390	15.867	0.0040	0.0703
1.50	1.419	15.883	0.0090	0.1563
1.70	1.442	15.896	0.0139	0.2366
2.00	1.447	15.916	0.0226	0.3760

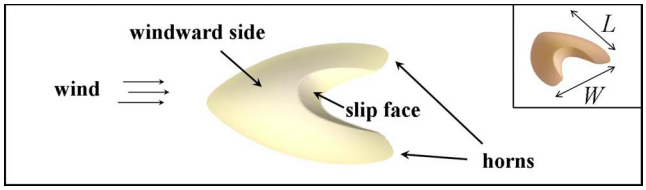

FIG. 4. (Color online) Sketch of a barchan dune showing the windward side, horns, and slip face. In the inset we see the definitions of dune width W and length L.

The wind velocity u_* in the dune fields on Mars is an unknown quantity. It must be determined from the calculations of dunes, as we will see in the next section. Indeed, there is still one missing quantity for Mars which we need in order to solve the sand transport equations: γ, which appears in Eq. (10). γ is given by the product $r\tilde{\gamma}$, where $r=|\vec{v}_s|/\Delta v_{hor}$ is related to the saltation trajectories, and $\tilde{\gamma}$ [Eq. (6)] gives the strength of the soil erosion. However, r and $\tilde{\gamma}$ cannot be calculated separately [13]. It is the quantity γ [Eqs. (10) and (11)] that can be determined from comparison with measurements of the transient of flux saturation. The terrestrial value $\gamma=0.2$ has been obtained by Sauermann *et al.* [13] from comparison of the saturation transient of the flux with experimental and numerical data [35,37,36], which are not available for Mars. Therefore γ is the parameter of the saltation model that remains to be determined for saltation transport on Mars. It will be obtained in the next section, from the calculations of Martian barchan dunes.

IV. DUNE FORMATION ON MARS

One very common type of dunes on Mars are *barchans*. They have one slip face and two horns, and propagate on bedrock under conditions of unidirectional wind (Fig. 4). Barchans are the simplest and best known dunes [7,38]. They are the subject of scientific and also environmental interest because of their high migration speed: on Earth, barchans 1–5 m high may cover 30–100 m in a year.

On Mars, barchan dunes occur on the floor of craters and on the north pole [38]. Similarly to Earth's barchans, they form corridors and large dune fields, as in the Arkhangelsky crater [Fig. 1(a)]. It appears surprising that intracrater dunes on Mars look in general similar: they have mostly an elongated shape [38].

The barchan dunes in the Arkhangelsky crater (41.0°S, 25.0°W) are among the largest barchans on Mars. Further, there are good reasons to begin our study of Martian barchans with the Arkhangelsky dunes: they have a wide spectrum of dune sizes; have not been significantly altered by secondary winds; and do not appear joined at their horns forming chains of barchanoids. For example, such features are observed in the dunes at Kaiser crater and Proctor crater [30].

Let us try to reproduce the shape of the Arkhangelsky barchans with the dune model using parameters of the present atmosphere of Mars. The atmospheric pressure P and temperature T near the Arkhangelsky crater are, respectively,

5.5 mbar and 210 K [27]. These values yield a local Martian atmospheric density $\rho_{\text{fluid}}=0.014\ \text{kg/m}^3$, and a fluid viscosity $\eta\approx 1.06\ \text{kg/m s}$. Using the mean grain diameter $d=500\ \mu\text{m}$, grain density $\rho_{\text{grain}}=3200\ \text{kg/m}^3$, and gravity $3.71\ \text{m/s}^2$, it follows that the threshold wind friction speed for saltation in the Arkhangelsky crater is $u_{*\text{t}}=2.12\ \text{m/s}$. In this manner, all parameters of the saltation model, but γ [Eq. (11)], are determined using the equations presented in the previous section.

A. Shape of the Arkhangelsky barchans

In the calculations of barchans, a constant upwind shear velocity $u_*>u_{*\text{t}}$ and a small influx $q_{\text{in}}/q_{\text{s}}$ (the interdune flux) are imposed in x (downwind) direction at the inlet, starting with a Gaussian hill having volume similar to the dune we want to reproduce. The hill evolves in time until displaying the barchan *shape*, i.e., linear relations between length L, width W, and height H [12,39].

Measured values of shear velocity of Martian winds are mostly between 0.4 and 0.6 m/s [40], which are much lower values than the Martian threshold for saltation ($\approx$2.0 m/s). Indeed, many authors estimated that the shear velocity u_* of Martian sand-moving winds, which occur within gusts of extreme dust storms, may reach maximum values between 2.2 and 4.0 m/s [4,6]. Again, very unprobably u_* must achieve values of the order of 4.0 m/s on Mars [5].

On the other hand, we know from experience with terrestrial dune fields that the flux in areas between dunes is normally small, between 10% and 40% of the maximum flux q_{s} [26]. Moreover, as shown from calculations in previous work, the shape of a barchan dune of given size depends in an important manner on the interdune flux only for values of $q_{\text{in}}/q_{\text{s}}$ above this range [39].

On the basis of the observations above, we try to reproduce, first, the shape of *one* Arkhangelsky barchan, which has width $W\approx 650$ m, using $q_{\text{in}}/q_{\text{s}}=20\%$. Furthermore, we take values of wind friction speed in the maximum range between 2.0 and 4.0 m/s, which gives $u_*/u_{*\text{t}}$ approximately between 1.0 and 2.0 in the Arkhangelsky crater. Now the quantity γ remains [Eq. (11)]. As a first guess, we take the terrestrial value $\gamma=0.2$ and investigate whether the Arkhangelsky dune can be obtained with u_* in the above-mentioned range.

We obtained a surprising result: if we take the same $\gamma=0.2$ as on Earth, the Gaussian hill does not evolve into a barchan: a *dome* is obtained, i.e., a dune that has no slip face. In fact, domes appear when dunes are too small to develop the slip face characteristic of barchans [12]. However, if we take γ_{Mars} on Mars of the order of ten times the terrestrial value $\gamma_{\text{Earth}}=0.2$, then barchan dunes with shape similar to the Arkhangelsky barchan can be obtained, as we see in Fig. 5: the elongated shape characteristic of the Arkhangelsky dunes is a result of low values of shear velocity, with $u_*/u_{*\text{t}}$ smaller than 1.5. This means values of u_* up to 3.0 m/s. For a constant value of $\gamma=2.0$, the dune shape deviates from the Arkhangelsky barchans for increasing values of u_*. Thus the shear velocity in the Arkhangelsky crater must be close to the threshold for saltation transport. This explains the elongated shape of intracrater barchan dunes on Mars.

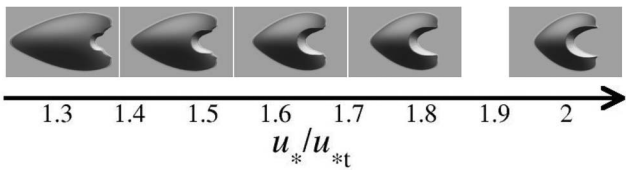

FIG. 5. Barchan dunes of width $W=650$ m calculated using parameters for Mars, with $\gamma=10\gamma_{\text{Earth}}$, and different values of wind shear velocity $u_*/u_{*\text{t}}$.

B. Entrainment of saltating grains on Mars

The wind shear velocity $u_*\approx 3.0$ m/s estimated for the Arkhangelsky crater is well within predicted maximum values of u_* on Mars; but why should the Martian γ [Eq. (11)] be ten times larger than on Earth?

The quantity $r=\gamma/\tilde{\gamma}$ [Eq. (11)] on Mars should not differ much from Earth's value. This is because the ejection velocity of splashed grains is proportional to the velocity of the average impacting grains [41], which in turn scales with the average saltation velocity v_{s}. In this manner, we must understand why the Martian entrainment rate, $\tilde{\gamma}$, differs from the one on Earth. This quantity determines the intensity of the grain-bed collisions, the modeling of which is beyond the scope of this work [13].

However, Anderson and Haff [41] showed that the number of splashed grains is proportional to the velocity v_{imp} of the impacting grains (and thus to v_{s}). In a previous work, we have proposed a scaling relation for γ based on the proportionality between the number of splashed grains and the grain velocity [39]. By rescaling v_{s} with $v_{\text{esc}}=\sqrt{gd}$, which is the velocity necessary to escape from the sand bed [42], we arrive at $\tilde{\gamma}\propto v_{\text{s}}/\sqrt{gd}$. However, v_{s} scales with $u_{*\text{t}}$ and has only a very weak dependence on u_*, as we can see in Table II. In this manner, we obtain $\tilde{\gamma}\propto u_{*\text{t}}/\sqrt{gd}$ [39]. From the values of the parameters on Earth, we obtain that the constant of proportionality is approximately 0.045 [17]. Thus the following equation for γ is obtained [17]:

$$\gamma=0.045\frac{u_{*\text{t}}}{\sqrt{gd}}. \tag{14}$$

Equation (14) gives $\gamma\approx 2.24$ in the Arkhangelsky crater, which is in fact one order of magnitude higher than the Earth's value, as obtained in a different way from the calculations in Fig. 5.

Summarizing, we found that the entrainment rate of grains into saltation on Mars is ten times higher than on Earth. This is explained by the Martian larger splash events, which are a consequence of the higher average velocity of saltating grains on Mars.

What is the consequence of a ten times higher entrainment rate on Mars? Because the saturation length of the sand flux depends on the rate at which grains enter saltation, the larger splash events on Mars have a crucial implication for the formation of sand dunes on the red planet.

While on one hand the lower Martian atmospheric density ρ_{fluid} and gravity g result in longer grain trajectories than on

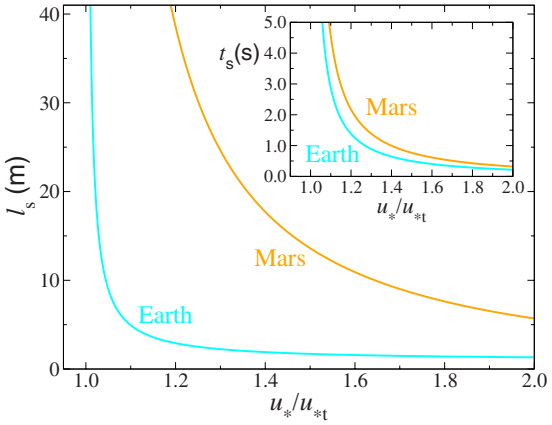

FIG. 6. (Color online) Main plot: characteristic length of flux saturation, ℓ_s, calculated with Eq. (10), as a function of u_*/u_{*t}. The inset shows the characteristic time $t_s=\ell_s/v_s$ as a function of u_*/u_{*t}, where v_s is the average grain velocity [Eq. (B3)].

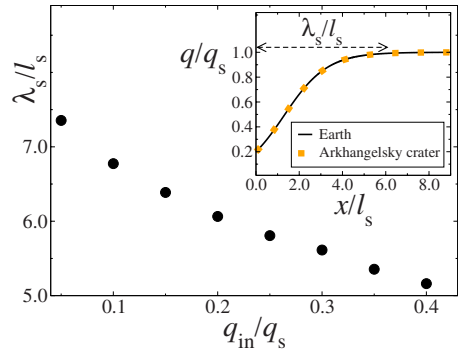

FIG. 7. (Color online) Sand flux calculated over a flat sand bed on Mars and on Earth. Main plot: distance of flux saturation, λ_s, normalized by the characteristic length ℓ_s, as a function of the influx q_{in}/q_s at the inlet. Inset: evolution of the normalized flux q/q_s with downwind distance x/ℓ_s for $q_{in}/q_s=0.20$.

Earth [9], the saturation transient of the flux on Mars is shortened by the faster increase in the population of saltating grains. This is because the wind strength is reduced more rapidly the faster the grains are launched into saltation after splash ("feedback effect" [11]). In fact, the characteristic length of flux saturation, ℓ_s [Eq. (10)], scales with the average saltation length, ℓ. However, ℓ_s is, furthermore, proportional to $1/\tilde{\gamma}$.

The characteristic length of flux saturation, ℓ_s, is calculated in the main plot of Fig. 6 using parameters for Earth and for the Arkhangelsky crater on Mars, with u_*/u_{*t} in the range between 1.0 and 2.0. In this figure, the Martian ℓ_s has been calculated using Eq. (10) with γ given by Eq. (14). In the inset of Fig. 6, we have calculated the characteristic time of flux saturation, $t_s=\ell_s/v_s$, for different values of u_*/u_{*t}.

It is remarkable that although the Martian and terrestrial values of ℓ_s differ by a factor of 10, t_s on Mars is nearly the same as the terrestrial one for a given u_*/u_{*t}. This is because the average velocity of saltating grains, v_s, is one order of magnitude higher on Mars, as shown in Sec. III.

As an example, we calculate the sand flux q [Eq. (9)], over a flat sand bed submitted to a unidirectional wind of constant strength, using parameters for Earth and for the Arkhangelsky crater on Mars. A constant influx q_{in}/q_s is set at the inlet. The evolution of the normalized sand flux q/q_s with the downwind distance x/ℓ_s calculated using parameters for Earth (line) and for the Arkhangelsky crater (symbols) is shown in the inset of Fig. 7 with $q_{in}/q_s=0.2$. In the main plot of Fig. 7, we see that it takes a distance λ_s of about six times ℓ_s, from the edge of the sand bed, for the sand flux to achieve 99% of its saturated value q_s, using realistic values of q_{in}/q_s between 0.1 and 0.4.

If we take, for instance, $u_*/u_{*t}=1.50$, then we obtain, with Eq. (10), $\ell_s=0.71$ and 13.62 m on Earth, respectively, in the Arkhangelsky crater. On the basis of Fig. 7, this leads to $\lambda_s \approx 4.3$ m on Earth, while the Martian λ_s is approximately 81 m. Furthermore, flux saturation is reached within approximately $6t_s$, i.e., within 3.0 s on Earth and 4.6 s on Mars. However, if we had taken the terrestrial $\gamma=0.2$ for Mars, then the values of Martian flux transient length and time obtained would be of the order of 100, respectively, 10 times larger than the terrestrial ones.

The larger value of γ on Mars shortens the characteristic distance of flux saturation [Eq. (10)] by one order of magnitude. However, since dunes cannot be smaller than the saturation length, this means that the scale of dunes that is predicted from the scaling of the flux saturation distance with the average saltation length, ℓ [43], is reduced by a factor of 10. In conclusion, the Martian larger splash is the missing link to understand the size of Martian dunes formed by the thin atmosphere of the red planet.

C. Friction speed of Martian sand-moving winds

In the calculations of Fig. 5, we could estimate the shear velocity u_*/u_{*t} from comparison with the shape of one selected barchan in the field, taking $\gamma_{Mars}=10\gamma_{Earth}$ and assuming a given value of the interdune flux q_{in}/q_s in the Arkhangelsky crater. However, since γ can be now *calculated* for different atmospheric conditions, we can solve the model equations to find the values of u_*/u_{*t} and q_{in}/q_s at a given dune field on Mars. Indeed, both field variables can be obtained from comparison with the *minimal dune*, as explained in Ref. [39].

In order to develop the slip face characteristic of barchans, sand hills must reach a minimum size, below which they are called *domes*. We have found that the minimal dune width W_{min} is around $13\ell_s$, and is approximately independent of the interdune flux, q_{in}/q_s [39]. In this manner, W_{min} yields, through Eq. (10), the value of u_*/u_{*t} at a given dune field. Moreover, once u_*/u_{*t} is determined, the value of q_{in}/q_s can be obtained from the shape of the minimal dune: the eccentricity L_{min}/W_{min} decreases approximately linearly with q_{in}/q_s [39].

In the preceding paper [17], we have applied the method of the minimal dune size to obtain the wind velocity and interdune flux in different Mars dune fields. In the present work, our aim is to present in detail the calculations of that paper and to discuss the implications of the outcomes for the formation and evolution of dunes on the present Mars.

In the Arkhangelsky crater on Mars [Fig. 1(a)], the minimal dune is indicated by two domes which have width

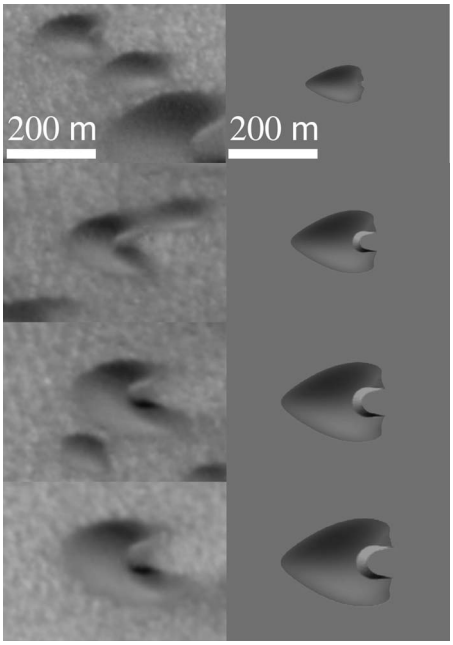

FIG. 8. Calculations of Martian north polar barchans near 77.6°N, 103.6°W [Fig. 1(b)]. We see MOC images of dunes of different sizes on the left, and on the right we see dunes calculated using $P=8.0$ mbar, $T=190$ K, $u_*=2.92$ m/s, and $q_{in}/q_s=0.29$. Images courtesy of NASA/JPL/MSSS.

$W_{min}\approx 200$ m and length $L_{min}\approx 400$ m. From $W_{min}=200$ m, we obtain $\ell_s\approx 15.5$ m, which gives $u_*/u_{*t}\approx 1.45$ or $u_*\approx 3.07$ m/s in the Arkhangelsky crater. This is essentially the same result obtained previously from comparison with the elongated shape (Fig. 5). Next, using this shear velocity, we calculate the eccentricity L_{min}/W_{min} of the minimal "Arkhangelsky" dune as a function of q_{in}/q_s, as described in Ref. [39]. We find that the ratio $L_{min}/W_{min}\approx 2.0$ is obtained with an average interdune flux $q_{in}\approx 25\%$ of the saturated flux q_s. Again, this value is nearly the same interdune flux assumed in the calculations of Fig. 5. In Ref. [17] we have compared calculated dunes with Arkhangelsky barchans of different sizes observed in the MOC images.

Let us study a second Martian barchan field which is near the north pole [Fig. 1(b)]. At the location of the field, in which $W_{min}\approx 80$ m and $L_{min}\approx 130$ m, $P=8.0$ mbar and $T=190$ K [27], and thus $u_{*t}\approx 1.62$ m/s. From the minimal dune width $W_{min}=80$ m, we obtain $u_*/u_{*t}\approx 1.8$ or $u_*=2.92$ m/s using Eq. (10). Further, from the eccentricity of the minimal dune, $L_{min}/W_{min}\approx 1.6$, we obtain $q_{in}/q_s=0.30$. In Fig. 8 we see images of north polar dunes of different sizes together with the dunes calculated using parameters for the field studied.

It is interesting that the shear velocity u_* obtained for the north polar field is nearly the same as the one in the Arkhangelsky crater, i.e., $u_*\approx 3.0$ m/s, although u_{*t} is lower in the north polar field. The values of u_*/u_{*t} and q_{in}/q_s obtained for the Arkhangelsky barchans and for the north polar dunes are within the range of the ones measured in terrestrial barchan fields [14,34,44], and reproduce not only the minimal dune but also describe well the dependence of the shape on the dune size in both Martian fields studied [Fig. 9(a)].

D. Dune height and migration velocity of barchans

So far we have used the model to obtain information about wind and flux conditions in the field based on the dune shape observed in the images. From the MOC images, we could only measure the length and the width of the dunes. In fact, measuring the height of Martian dunes is still one of the

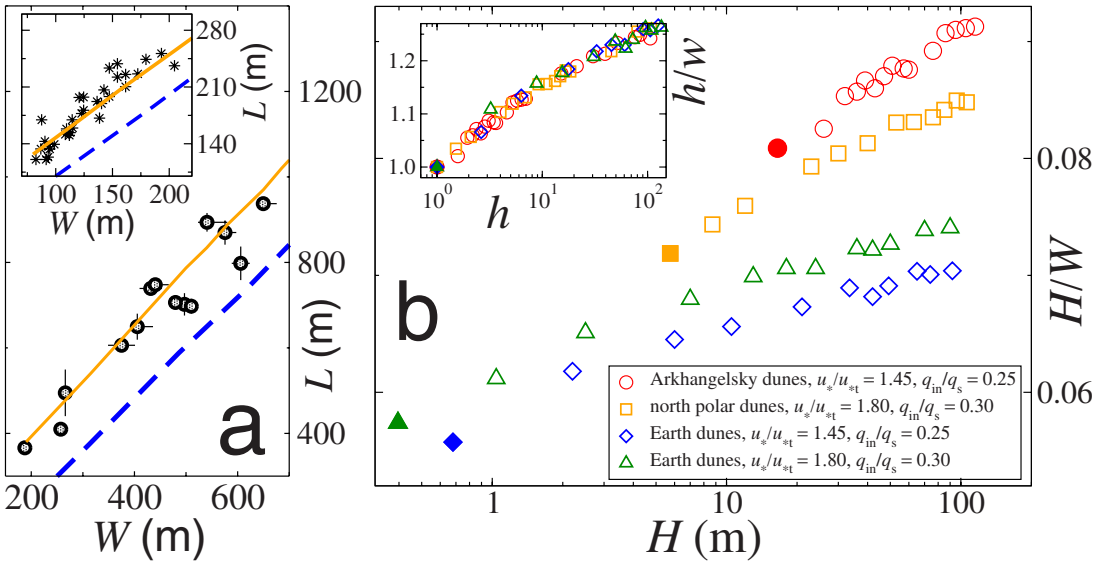

FIG. 9. (Color online) (a) Main plot: length L vs width W of the Arkhangelsky barchans (circles) together with calculation results (straight line) obtained with parameters for that field. The dashed line shows L vs W for terrestrial dunes obtained with $u_*/u_{*t}=1.45$ and $q_{in}/q_s=0.25$. In the inset we see L vs W of the north polar dunes (stars) together with calculations (straight line), while the dashed line corresponds to terrestrial dunes obtained with $u_*/u_{*t}=1.80$ and $q_{in}/q_s=0.30$. (b) Main plot: aspect ratio H/W vs dune height H of barchan dunes on Mars and on Earth. For each curve, the minimal dune is indicated by the filled symbol. All curves displayed in the main plot are shown again in the inset but in terms of the normalized height $h\equiv H/H_{min}$ and width $w\equiv W/W_{min}$.

TABLE III. The table shows the height H_{min}, width W_{min}, length L_{min}, volume V_{min}, and migration velocity v_0, of the minimal dune on the Martian fields of Figs. 1(a) and 1(b). The corresponding values for the minimal dune on Earth obtained with the Martian u_*/u_{*t} and q_{in}/q_s are also shown in the table.

	$u_*/u_{*t}=1.45$ $q_{in}/q_s=0.25$		$u_*/u_{*t}=1.80$ $q_{in}/q_s=0.30$	
Minimal dune	Mars [Fig. 1(a)]	Earth	Mars [Fig. 1(b)]	Earth
H_{min} (m)	16.5	0.69	5.8	0.39
W_{min} (m)	204	12.2	80	6.9
L_{min} (m)	400	19.2	127	9.2
V_{min} (m^3)	400 000	50	19 500	7.5
v_0 (m/year)	400	560	1750	2160

most challenging problems, and has been the subject of intense research in the last few years [45].

The ratio H/W of the dunes at the Arkhangelsky crater and in the north polar field as predicted from the model is shown in the main plot of Fig. 9(b). In the same figure, we also show the behavior of H/W for terrestrial dunes calculated with the same u_*/u_{*t} and q_{in}/q_s obtained for the Martian dunes. The filled symbols identify the corresponding minimal dune in each field. We see that the smallest barchans on Mars have height H_{min} of the order of 10 m (Table III) and are, thus, almost 20 times larger than the smallest barchans on Earth [46]. The inset of Fig. 9(b) shows the same curves of the main plot in terms of the normalized height, $h=H/H_{min}$ and width, $w=W/W_{min}$. We see that h/w vs h of all curves behave in a similar manner, independently of wind speed, sand influx, and atmospheric conditions.

Using the dune model, it is also possible to predict the migration velocity of barchans in a given dune field on Mars. The calculation of the velocity of the barchans studied in this work is shown in Fig. 10. In the main plot of this figure we show the dune velocity v as a function of the dune length L on Mars and on Earth. We see that Mars dunes move typically ten times faster than Earth dunes of the same L, obtained with similar values of u_*/u_{*t} as on Mars.

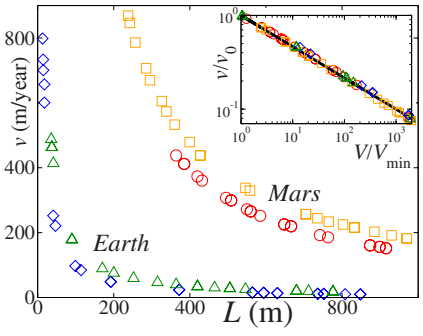

FIG. 10. (Color online) Dune velocity v as a function of the length L of the dunes calculated in Fig. 9(b). In the inset, the dune velocity normalized with the velocity of the minimal dune, v_0, is shown as a function of the normalized dune volume, V/V_{min}, where V_{min} is the volume of the minimal dune. The straight line in the inset corresponds to the equation $v/v_0=(V/V_{min})^{-1/3}$.

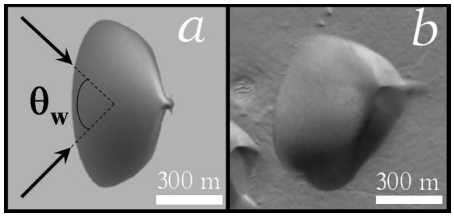

FIG. 11. Calculation of the dunes at Wirtz crater [Fig. 1(c)]. In (a) we see one calculated dune, while in (b) we see an image of one dune at the Wirtz crater (image courtesy of NASA/JPL/MSSS). Arrows indicate the wind directions, with $\theta_w=100°$ and $T_w=2.9$ days. Simulation snapshot in (a) corresponds to $t=15$ years after having started a calculation with a Gaussian hill with nearly the same volume of the bimodal dune shown in the figure. The Dune shape does not appear to change in time.

The migration velocity of barchan dunes scales with $Q/V^{1/3}$, where $Q\equiv q_s/\rho_{sand}$ and V is the dune volume. In this manner, Martian dunes migrate faster than Earth dunes because of the higher values of q_s on Mars (Table II). Let us normalize the dune velocity v with the migration velocity of the minimal dune, v_0. In the inset of Fig. 10, we show the behavior of v/v_0 as a function of V/V_{min}, where V_{min} is the volume of the minimal dune. We see that the equation $v/v_0=(V/V_{min})^{-1/3}$, which corresponds to the straight line in the plot, captures well the behavior of all Martian and terrestrial curves.

The calculations show that for a given u_*/u_{*t}, the smallest Martian barchans would move nearly as fast as the smallest dunes on Earth (Table III). However, winds on Mars are only seldom above the threshold for saltation [4,6,40]. As reported from observations of Mars missions, saltation transport on Mars occurs during a few seconds in time intervals of several years. If, for example, winds on Mars achieve $u_*\approx 3.0$ m/s during 40 s every 5 years [6], then, from Fig. 10, we see that a Martian barchan of length 200 m would need 5 years $\times 10^{-3}/(3600\times 24\times 365)/40\approx 4000$ years to move 1.0 m.

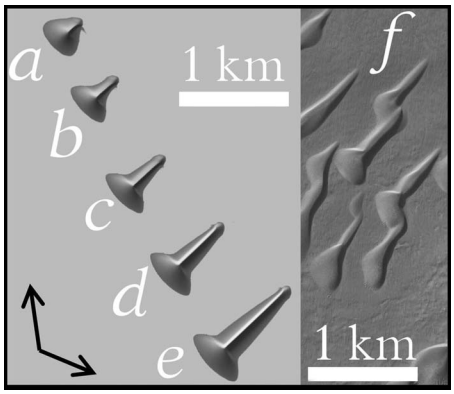

FIG. 12. Dunes at 49.6°S, 352.9° W on Mars [Fig. 1(d)]. On the left we see snapshots of the calculation at $t=2.7$ (a), 6.6 (b), 14.5 (c), 24 (d), and 39 months (e) after starting with a sand hill at $t=0$. $\theta_w=140°$ and $T_w=5.8$ days. Wind directions are indicated by the arrows. An image of the dunes is shown on the right (f). Image courtesy of NASA/JPL/MSSS.

TABLE IV. Main quantities controlling saltation on Mars. For each dune field in Fig. 1, the fluid density ρ_{fluid} and the threshold u_{*t} are calculated from the local pressure P and temperature T which are taken from Ref. [27]. Next, γ is calculated with Eq. (14). While the shear velocity u_* at the fields in Figs. 1(a) and 1(b) is calculated from the dune shape, the value $u_*=3.0$ m/s has been used to obtain the dunes in Figs. 1(c)–1(e). For each dune field, the grain velocity v_s and the saturated flux q_s are obtained with Eq. (B3), respectively, with Eq. (8) using the corresponding value of u_* displayed in the table.

Field	Location	P (mbar)	T (K)	ρ_{fluid} (kg/m^3)	u_{*t} (m/s)	γ	u_* (m/s)	v_s (m/s)	q_s (kg/m s)
Fig. 1(a)	41.0°S, 25.0° W	5.5	210	0.014	2.12	2.24	3.07	17.8	0.147
Fig. 1(b)	77.6°N, 103.6° W	8.0	190	0.022	1.62	1.71	2.92	12.3	0.240
Fig. 1(c)	48.6°S, 25.5° W	5.5	175	0.017	1.89	1.99	3.00	14.6	0.189
Fig. 1(d)	49.6°S, 352.9° W	5.0	185	0.014	2.06	2.17	3.00	16.5	0.148
Fig. 1(e)	76.4°N, 272.9° W	8.5	150	0.030	1.35	1.43	3.00	9.2	0.376

This result explains why spacecrafts orbiting Mars never revealed any movement of Martian barchan dunes.

E. Martian bimodal sand dunes

Because linear and star dunes like the ones found on Earth were almost not observed in the first images of Mars taken by Mariner 9 and Viking orbiters, it has been suggested that nonunimodal wind regimes should be very rare on Mars [47]. However, the Mars Global Surveyor MOC camera has, more recently, imaged a high diversity of dune shapes that had been never observed in images of previous missions.

On bedrock and in areas of low sand availability, there appear many exotic and up to now unexplained dune forms where barchans should occur if the wind regime were unidirectional. Dunes as those in Figs. 1(c)–1(e) cannot appear in areas of unidirectional winds, for in this case barchans should be formed. Indeed, it is possible to recognize in the images of Figs. 1(c)–1(e) that the dominant winds define a resultant direction.

As reported in the preceding paper [17], we found that the dune shapes in Figs. 1(c)–1(e) can be obtained with a *bimodal* wind regime. Here our aim is to extend the presentation of the calculations of bimodal dunes published in that paper, and to discuss the implications of our findings for the understanding of the Martian wind regimes.

In our calculations, the wind alternates its direction periodically forming an angle θ_w as sketched in Fig. 11(a). The wind lasts a time T_w at both directions. In both directions the wind strength is the same, namely $u_*=3.0$ m/s, as found from the calculations of barchan dunes. The change of wind direction is simulated through rotation of the field by an angle θ_w, keeping the wind direction constant. The separation bubble adapts to the wind direction after rotation of the field. As in the calculations of barchan dunes, we use open boundaries with a constant influx between 20% and 40% of q_s at the inlet, and the initial condition is a Gaussian hill whose volume is taken according to the volume of the dune. The quantities controlling saltation in each field are shown in Table IV.

The study of the morphology of bimodal dunes is not in the scope of the present work. In a future publication, we will show that the Martian dune shapes in Figs. 1(c)–1(e) appear within a wide spectrum of dune morphologies defined by the angle θ_w and the characteristic time T_w [48].

We obtain the dune shapes in Figs. 1(c)–1(e) using values of θ_w larger than 100° [17]. If $\theta_w \approx 100°$, then the dune shape in Fig. 11 is achieved; and for θ_w of the order of 120° or larger, dune forms as those in Fig. 12 are obtained, which elongate in time. As $\theta_w \to 180°$, a dune form of alternating slip face position appears.

All dune shapes in Figs. 11–13 have been achieved with a time T_w in the range of 0.7–5.8 days. If the period is too large, of the order of a few months, then the dunes evolve into barchanoidal forms.

The dune shape in Fig. 11 has been obtained with $\theta_w=100°$ and with $T_w=250\,000$ s ≈ 2.9 days, while $\theta_w=140°$ and $T_w=500\,000$ s ≈ 5.8 days has been used to calculate the dune in Fig. 12. Moreover, we found that the structure observed in the dune field of Fig. 1(e) can be obtained by a *change* in the local wind regime. The dune shape in Fig. 13 has been obtained in the following manner: (i) first, an elongated dune form as the one in Fig. 12 is formed with an angle $\theta_w=120°$ and with $T_w=60\,000$ s ≈ 0.7 day; and (ii) next, the angle θ_w has been reduced to 80°. Thereafter, the linear dune becomes unstable and decays into a string of rounded barchans as seen in Figs. 13(a)–13(d).

It is interesting to notice that our calculations provide a different explanation for the formation of the Martian dune field in Fig. 1(e) than that proposed by Bourke [49]. We found that the field in Fig. 1(e) consists of linear dunes which are decaying into barchans, while Bourke [49] sug-

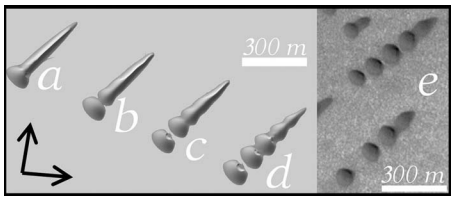

FIG. 13. Calculation of Martian north polar dunes at 76.4°N, 272.9° W [Fig. 1(e)]. First, an elongated dune is formed from a Gaussian hill after 2.5 months with $\theta_w=120°$ and $T_w=0.7$ day. Next, θ_w is shifted to 80° ($t=0$) giving rise to the dunes shown on the left, which correspond to snapshots at $t=5$ (a), 14 (b), 27 (c) and 45 days (d). Arrows indicate the wind directions. Dunes are about 8 m high. On the right (e) we see an image of the north polar dunes (image courtesy of NASA/JPL/MSSS).

gested an alternative view: the small barchans would merge to form the linear dunes.

The results of Figs. 11–13 provide evidence for bimodal wind regimes on Mars. We find that a variety Martian dune forms which appear in craters and which develop on bedrock have been formed by a wind whose direction alternates between two main orientations. We conclude that if more sand were available in those places, longitudinal dunes would in fact appear as observed in terrestrial sand seas. The study of the shape of linear dunes is the subject of a future publication [48].

Again, the wind strength $u_*=3.0$ m/s used in the calculations must be interpreted as the representative value of shear velocity that is above the threshold for saltation and is responsible for the major changes of the surface [5]. Because Martian winds are most of the time *below* the threshold for saltation, we expect the time scale T_{real} of the changes in wind directions to be in reality much larger than the values of T_{w} (a few days) found in the calculations.

We define as f_{w} the fraction of time the wind strength is above the threshold for saltation. From the results of the calculations of barchans, this means that the Martian u_* is around 3.0 m/s a fraction f_{w} of time. We interpret this value of shear velocity as the representative wind friction speed associated with the gusts of aeolian activity that occur during the strongest dust storms on Mars [4]. Further, the real time scale T_{real} of the changes in wind direction is defined through the relation $f_{\mathrm{w}}=T_{\mathrm{w}}/T_{\mathrm{real}}$.

Let us assume that winds above the threshold on Mars occur generally during $\Delta t_{\mathrm{saltation}}=40$ s at intervals of $\Delta T=5$ years (2000 days or 1.728×10^8 s) [4,6], i.e., $f_{\mathrm{w}}=\Delta t_{\mathrm{saltation}}/\Delta T\approx2.31\times10^{-7}$. A characteristic time $T_{\mathrm{w}}\approx1-5$ days means $T_{\mathrm{w}}=86\,400-432\,000$ s. Dividing T_{w} by $\Delta t_{\mathrm{saltation}}=40$ s, this characteristic time corresponds to 2160–10 800 gusts of saltation transport. The Martian real time T_{real} is

$$T_{\mathrm{real}}=\frac{T_{\mathrm{w}}}{\Delta t_{\mathrm{saltation}}}\times 5.0\ \text{years}\approx 10\,800-54\,000\ \text{years}. \tag{15}$$

Therefore the real time of oscillation of the direction of sand-moving winds on Mars found from our calculations is of the order of 10^4 years, where it has been assumed that Martian saltation occurs as frequently as observed from the Mars Missions [4–6].

V. DISCUSSION AND CONCLUSIONS

In the present work, we have applied a well-established dune model, which successfully reproduces the shape of terrestrial dunes measured in the field, to study dune formation on Mars. We presented in detail the calculations of Mars dunes published in a recent paper (Ref. [17]) showing also how the quantities controlling saltation on Mars are obtained from the model equations. We also discussed the implications of the calculation results for the Martian wind regimes and migration velocity of Mars dunes. In summary, we found that dunes observed in the images of Mars could have been formed by the action of sand-moving winds that occur occasionally under the present atmospheric conditions of the red planet. Below we give a list of the main conclusions.

(1) The quantities controlling Martian saltation, such as the average grain velocity, mean saltation height, and saturated flux, may vary in a significant manner depending on the location on Mars. This is because local average values of Martian surface pressure and temperature may be very different depending on the geographical location.

(2) From the shape of barchan dunes on Mars, we found that the rate at which Martian grains enter saltation is ten times higher than on Earth. The Martian higher entrainment rate, which is a result of the larger splash events on Mars, shortens the length of flux saturation and reduces the scale of dunes that is obtained if only the Martian larger saltation length is considered [43,46].

(3) All dune shapes studied in this work could be reproduced with values of shear velocity that do not exceed $u_*=3.0\pm0.1$ m/s, independently of the location on Mars. We interpret this value as the representative friction speed of sand-moving winds that occur during the strongest dust storms on Mars.

(4) For the same value of relative wind velocity $u_*/u_{*\mathrm{t}}$, barchans would move ten times faster on Mars than on Earth. However, the migration velocity of Martian barchans is negligible because saltation transport in fact occurs only seldom on the present Mars.

(5) We found Martian dune shapes that have been formed by bimodal wind regimes. The time scale of changes in wind direction obtained in calculations is of the order of a few days. Taking into account that winds transport sand on Mars during some tens of seconds in intervals of a few years [6], this time scale is in reality of the order of 10 000–50 000 terrestrial years.

It is interesting to notice that a significant change in wind direction (by 90° or more) is expected to occur after each extreme of the *orbital* cycle of Mars, which is determined by the combined effect of the precession of its axis and the arrival at *perihelion* [47,50–54]. Because of precession of the Martian axis, each pole of Mars appears tilted to the sun in a cycle of 51 000 years. Now the latitude which "looks" toward the sun at perihelion is 15°S, but this "subsolar latitude at perihelion" (SLP) migrates ±25° about the Equator over a 51 kYr time span [50]. This orbital cycle is the most important one for the climate of Mars, the hemisphere of the SLP having short, hot summers, and being the one of major dust storms activity. In 25 500 years, it is the northern hemisphere that will be tilted to the sun. "The large amounts of fine dust currently deposited in the northern hemisphere in regions such as Tharsis, Arabia, and Elysium will be redistributed to the southern hemisphere" [55]. This half cycle of 25 500 years is in fact well within the range of characteristic time $10\,800<T_{\mathrm{real}}<54\,000$ years of bimodal winds found from our calculations of sand dunes on Mars.

In comparison, the time scale T_{real} of changes in directions of bimodal winds in terrestrial dune fields is of the order of a few weeks or months. On Earth, linear dunes appear due to wind changes that occur *seasonally* [56,57], since the fraction of time f_{w} the wind friction speed u_* is above the threshold $u_{*\mathrm{t}}$ is much larger than on Mars [34,58]. In this manner,

we do not expect the wind changes due to precession of the Earth's axis to play a major role for the shape of terrestrial bimodal sand dunes. On the other hand, Martian winds that are not associated with the intense dust storms mentioned in the last paragraph are too weak to move sand. Indeed, such weak winds are responsible for the appearance of dust devils that leave ephemeral marks on the surface of Martian dunes [30], which appear unmobile. The presence of bimodal dunes on Mars can, thus, only give information on the oscillation of winds stronger than the threshold, and not on the common wind regime (under the threshold).

In conclusion, using the characteristics of sand dunes, the model can be applied in order to determine some properties of the Martian atmosphere or sediments, when they cannot be determined by other ways, or to confirm indirect measurements. One example of such application has been given in Ref. [59], in which the relevance of sand induration for the dune morphology at Chasma Boreale, in the Martian north polar region, was investigated with the help of simulations using the dune model. The model equations allow calculation of the migration velocity of active barchans or, for instance, the time required for a barchan to change its shape into a bimodal dune. Thus the model can be used in the future to estimate the age of dune fields on Mars, to predict their evolution, and to test hypotheses about their formation through comparison with simulations of entire dune fields such as those in Refs. [60,61].

Moreover, one important question is what is the typical size of the sediments that constitute Mars dunes. The dune shape and minimal size change with the grain diameter d. In fact, images sent from the rovers at the Meridiani Planum landing site revealed ripples composed by grains of diameter d around 100 μm [5,33,62], which is a much lower value than the one of the larger, dark intracrater dunes [29]. Thus while the calculations of the present work have been successfully performed using the value of grain diameter revealed for dark dunes [29], the model can be naturally adapted to investigate dunes in other locations where grain size and/or constitution are not known and can be determined through comparison of the dunes with simulation outcomes.

The shape of Martian dunes could be only achieved with real wind and atmospheric conditions of the present Mars because the entrainment rate of grains into saltation, which we found to be ten times higher on Mars than on Earth, was incorporated in the model equations. In fact, it is well-known from experiments that the splash events on Mars are much larger than on Earth due to the higher velocity of Martian grains [10]. What we have found in the calculations is the implication of the larger amount of splashed grains on Mars for the flux saturation and formation of dunes. It would be interesting to make a full microscopic simulation for the saltation mechanism of Mars similar to the one that was recently performed by Almeida *et al.* [63] to confirm our findings microscopically.

ACKNOWLEDGMENTS

We acknowledge the help of Orencio Durán in the formulation of the scaling relation for γ and in the calculations of the Arkhangelsky barchans. We thank Bruno Andreotti, Philippe Claudin,Volker Schatz, Haim Tsoar, and Kenneth Edgett, Günter Wunner, Harald Giessen, Jason Gallas, and Adriano Sousa for fruitful suggestions and valuable comments. This research was supported in part by Volkswagenstiftung and The Max-Planck Institute. E. J. R. Parteli acknowledges support from CAPES -Brasília/Brazil.

APPENDIX A: MEAN SALTATION TRAJECTORIES

The mean saltation length ℓ is defined in terms of the grain velocity $|\vec{v}|$ and of the initial vertical velocity, v_z^{eje} [13]:

$$\ell = v_z^{\mathrm{eje}}(2|\vec{v}|/g), \tag{A1}$$

where $v_z^{\mathrm{eje}}=\alpha\Delta v_{\mathrm{hor}}$, α is an effective restitution coefficient for the grain-bed interaction, and $\Delta v_{\mathrm{hor}}=v_{\mathrm{hor}}^{\mathrm{imp}}-v_{\mathrm{hor}}^{\mathrm{eje}}$ gives the difference between the horizontal velocities (in the direction of the flow) of the grains at the moment of impact, $v_{\mathrm{hor}}^{\mathrm{imp}}$, and at the moment of ejection, $v_{\mathrm{hor}}^{\mathrm{eje}}$.

APPENDIX B: AVERAGE VELOCITY OF THE SALTATING GRAINS

The velocity of the saltating grains, $\vec{v}$, is determined from the balance between three forces: (i) the drag force acting on the grains; (ii) the bed friction which yields the loss of momentum when the grains impact onto the ground, and (iii) the downhill force, which acts on the saltation layer in the presence of bed slopes. To calculate the grain velocity, we need to take into account the modification of the air flow due to the presence of the saltating grains. However, the model equations do not account for the complex velocity distribution within the saltation layer. Instead, a reference height z_1 is taken between the ground at the roughness height z_0^{sand} and the mean saltation height z_{m}, at which the "effective" wind velocity, $\vec{u}_{\mathrm{eff}}$, is calculated [13].

Finally, a useful approximation is employed which simplifies the equations in a significant manner and leads to only a negligible error [13]. In the model, the velocity $\vec{u}_{\mathrm{eff}}$ is calculated in the *steady state*, i.e., it is the *reduced* wind velocity within the saltation layer at saturation. In geomorphological applications, the sand flux over a dune is nearly everywhere saturated, with exception of those places where external variables change discontinuously, as, for instance, at a flow-separation, which occurs at the dune brink, or at a phase boundary bedrock-sand which occurs at the windward foot of a barchan dune. Therefore we can replace the density ρ which appears in the expression for the grain born shear stress τ_{g} with the saturated density $\rho_{\mathrm{s}}=(\tau-\tau_{\mathrm{t}})\ell/|\vec{v}|\Delta v_{\mathrm{hor}}$ [13]. The following expression is obtained, in this manner, for $\vec{u}_{\mathrm{eff}}$:

$$\vec{u}_{\mathrm{eff}} = \frac{u_{*\mathrm{t}}}{\kappa}\left\{\ln\frac{z_1}{z_0^{\mathrm{sand}}} + 2\left[\sqrt{1+\frac{z_1}{z_{\mathrm{m}}}\left(\frac{u_*^2}{u_{*\mathrm{t}}^2}-1\right)}-1\right]\right\}\frac{\vec{u}_*}{|\vec{u}_*|}. \tag{B1}$$

The grain velocity, $\vec{v}$, is, next, calculated numerically from the equation [13]:

$$\frac{3}{4}\frac{\rho_{\text{fluid}}}{\rho_{\text{grain}}}\frac{C_{\text{d}}}{d}(\vec{u}_{\text{eff}}-\vec{v})|\vec{u}_{\text{eff}}-\vec{v}|-\frac{g\vec{v}}{2\alpha|\vec{v}}-g\vec{\nabla}h=0, \quad \text{(B2)}$$

where C_{d} is the drag coefficient, and $\vec{u}_{\text{eff}}$ is calculated with Eq. (B1). In this manner, the grain velocity obtained from Eq. (B2) is in fact the *average grain velocity* at the steady state, $\vec{v}_{\text{s}}$, since $\vec{u}_{\text{eff}}$ is the reduced wind velocity after flux saturation has been achieved [13]. Moreover, the mean saltation length is also computed using $|\vec{v}|=|\vec{v}_{\text{s}}|$ in the stationary condition where the sand flux is in equilibrium. In this manner, the mass conservation equation is written in terms of the *sand flux* [Eq. (7)].

Equation (B2) can be analytically solved in the simple case of the two-dimensional flow over a sand bed, where the gravitational term can be disregarded, which gives [19]

$$v_{\text{s}}=u_{\text{eff}}-v_{\text{f}}^{*}. \quad \text{(B3)}$$

In Eq. (B3), the relative velocity in the equilibrium, v_{f}^{*}, is given by

$$v_{\text{f}}^{*}=\frac{v_{\text{f}}}{\sqrt{2\alpha}}=\sqrt{\frac{2}{3\alpha C_{\text{d}}}\left[\frac{(\rho_{\text{grain}}-\rho_{\text{fluid}})gd}{\rho_{\text{fluid}}}\right]}, \quad \text{(B4)}$$

where v_{f} is the falling velocity of the grains that is obtained from the balance between the gravitational and drag forces in the case of vertically falling particles [32].

APPENDIX C: MODEL PARAMETERS

The following quantities are needed in order to solve the model equations: the atmospheric density ρ_{fluid}, gravity g, grain diameter d, and density ρ_{grain}, whose values are found in the literature and are discussed in the next section; the impact threshold velocity for saltation, $u_{*\text{t}}$, and the drag coefficient C_{d}; the effective restitution coefficient α and the heights z_{m}, z_1, and z_0^{sand}; γ [Eq. (11)]; and the wind shear velocity u_*.

The *impact threshold velocity* $u_{*\text{t}}$ is about 80% of the threshold for aeolian entrainment, $u_{*\text{ft}}$ [7], which in turn is calculated as in Iversen and White [3]. This leads to the following equation for $u_{*\text{t}}$:

$$u_{*\text{t}}=0.8A\sqrt{\frac{(\rho_{\text{grain}}-\rho_{\text{fluid}})gd}{\rho_{\text{fluid}}}}, \quad \text{(C1)}$$

where A is called the Shields parameter, which depends on the shape and sorting of the grains and on the angle of internal friction [25]. The Shields parameter is calculated as in Iversen and White [3]:

$$A=0.129\left[\frac{(1+6.0\times10^{-7}/\rho_{\text{grain}}gd^{2.5})^{0.5}}{(1.928\,\text{Re}_{*\text{ft}}^{0.092}-1)^{0.5}}\right] \quad \text{(C2)}$$

for $0.03\leqslant \text{Re}_{*\text{ft}}\leqslant 10$ and

$$A=0.129(1+6.0\times10^{-7}/\rho_{\text{grain}}gd^{2.5})^{0.5}\times\{1-0.0858\exp[-0.0617(\text{Re}_{*\text{ft}}-10)]\} \quad \text{(C3)}$$

for $\text{Re}_{*\text{ft}}\geqslant 10$, where $\text{Re}_{*\text{ft}}$ is the friction Reynolds number $\text{Re}_{*\text{ft}}\equiv u_{*\text{ft}}d/\nu$, and the constant 6.0×10^{-7} has units of kg $\text{m}^{0.5}$ s^{-2}, while all other numbers are dimensionless. The kinematic viscosity ν is defined as η/ρ_{fluid}, where η is the dynamic viscosity. We notice that in contrast to ν, η depends only on the atmospheric temperature and composition.

The *drag coefficient* C_{d} is calculated using the relative velocity of the grains obtained from the momentum balance [Eq. (B4)]. In this manner, we obtain the following expression for the drag coefficient C_{d} [19]:

$$C_{\text{d}}=\frac{4}{3}\left(A_{\text{d}}+\sqrt{2\alpha}\frac{B_{\text{d}}}{S}\right)^2, \quad \text{(C4)}$$

where

$$S=\frac{d}{4\nu}\sqrt{\left[\frac{(\rho_{\text{grain}}-\rho_{\text{fluid}})gd}{\rho_{\text{fluid}}}\right]} \quad \text{(C5)}$$

is called the fluid-sediment parameter and A_{d} and B_{d} are constants that contain information about the sediment shape factor and roundness. Equation (C4) is valid for Reynolds numbers Re in the range $0.2<\text{Re}<127$, while $A_{\text{d}}=0.95$ and $B_{\text{d}}=5.12$ for typical applications when particle's shape and roundness are not known [32].

It appears surprising that the effective restitution coefficient α, which contains the information about the bed-friction and the trajectories of the grains, appears in the expression for the drag coefficient C_{d}. In fact, at saturation, the momentum loss of the grains due to the collisions with the sand-bed is compensated by the grain-born shear stress, i.e., the aeolian drag force on the particles. It is this information that is contained in α and which enters the drag coefficient C_{d}.

The parameters α, z_{m}, and z_1 are computed using the equations obtained by Durán and Herrmann [19], which incorporate the time scale

$$t_\nu\equiv(\nu/g^2)^{1/3} \quad \text{(C6)}$$

and the length scale

$$\ell_\nu\equiv\left[\frac{\nu^2\rho_{\text{fluid}}}{A^2g(\rho_{\text{grain}}-\rho_{\text{fluid}})}\right]^{1/3}. \quad \text{(C7)}$$

and allow one to calculate the model parameters for saltation in different physical environments:

$$z_1=35\ell_\nu, \quad \text{(C8)}$$

$$z_{\text{m}}=14u_{*\text{t}}t_\nu, \quad \text{(C9)}$$

$$z_0^{\text{sand}}=d/20. \quad \text{(C10)}$$

The last equation gives intermediate values between $d/30$ [7] and $d/8$ [42]. Finally, the effective restitution coefficient $\alpha=v_z^{\text{eje}}/\Delta v_{\text{hor}}$ is simply calculated with the formula [19]

$$\alpha=0.17d/\ell_\nu. \quad \text{(C11)}$$

It must be emphasized that α is not directly related to the bouncing behavior of the impacting grains. α relates the initial vertical velocity of the *splashed* grains with the horizontal velocity gain of the impacting grains. Further research is required in order to shed light on the dependence of the effective restitution coefficient of the splash with the fluid viscosity ν through the length scale ℓ_ν [19,42].

[1] C. S. Breed, M. J. Grolier, and J. F. McCauley, J. Geophys. Res. **84**, 8183 (1979).
[2] R. Greeley, R. Leach, B. White, J. D. Iversen, and J. Pollack, Geophys. Res. Lett. **7**, 121 (1980).
[3] J. D. Iversen and B. R. White, Sedimentology **29**, 111 (1982).
[4] H. J. Moore, J. Geophys. Res. **90**, 163 (1985).
[5] R. Sullivan *et al.*, Nature (London) **436**, 58 (2005).
[6] R. E. Arvidson, E. A. Guinness, H. J. Moore, J. Tillmann, and S. D. Wall, Science **222**, 463 (1983).
[7] R. A. Bagnold, *The Physics of Blown Sand and Desert Dunes* (Methuen, London, 1941).
[8] B. R. White, R. Greeley, J. D. Iversen, and J. B. Pollack, J. Geophys. Res. **81**, 5643 (1976).
[9] B. R. White, J. Geophys. Res. **84**, 4643 (1979).
[10] J. R. Marshall, J. Borucki, and C. Bratton, Proc. Lunar Planet. Sci. Conf. **29**, 1131 (1998).
[11] P. R. Owen, J. Fluid Mech. **20**, 225 (1964).
[12] K. Kroy, G. Sauermann, and H. J. Herrmann, Phys. Rev. E **66**, 031302 (2002).
[13] G. Sauermann, K. Kroy, and H. J. Herrmann, Phys. Rev. E **64**, 031305 (2001).
[14] G. Sauermann, J. S. Andrade, Jr., L. P. Maia, U. M. S. Costa, A. D. Araújo, and H. J. Herrmann, Geomorphology **54**, 245 (2003).
[15] V. Schwämmle and H. J. Herrmann, Nature (London) **426**, 619 (2003).
[16] O. Durán and H. J. Herrmann, Phys. Rev. Lett. **97**, 188001 (2006a).
[17] E. J. R. Parteli and H. J. Herrmann, Phys. Rev. Lett. **98**, 198001 (2007).
[18] V. Schwämmle and H. J. Herrmann, Eur. Phys. J. E **16**, 57 (2005).
[19] O. Durán and H. J. Herrmann, J. Stat. Mech.: Theory Exp. (2006b) P07011.
[20] R. Sullivan, R. Greeley, M. Kraft, G. Wilson, M. Golombek, K. Herkenhoff, J. Murphy, and P. Smith, J. Geophys. Res. **105**, 24547 (2000).
[21] K. Pye and H. Tsoar, *Aeolian Sand and Sand Dunes* (Unwin Hyman, London, 1990).
[22] K. R. Rasmussen, J. D. Iversen, and P. Rautahemio, Geomorphology **17**, 19 (1996).
[23] We acknowledge an anonymous referee for this remark.
[24] W. S. Weng, J. C. R. Hunt, D. J. Carruthers, A. Warren, G. F. S. Wiggs, I. Livingstone, and I. Castro, Acta Mech. **2**, 1 (1991).
[25] A. Shields, California Institute of Technology, Technical Report Publ. No. 167, 1936 (unpublished).
[26] S. G. Fryberger, A. M. Al-Sari, T. J. Clisham, S. A. R. Rizvi, and K. G. Al-Hinai, Sedimentology **31**, 413 (1984).
[27] MGSRS, Mars Global Surveyor Radio Science Team, 2006, "Late Martian Weather," http://nova.stanford.edu/projects/mgs/.
[28] Crane Company, Technical Paper No. 410, 1988 (unpublished); Also http://www.lmnoeng.com/Flow/GasViscosity.htm.
[29] K. S. Edgett and P. R. Christensen, J. Geophys. Res. **96**, 22765 (1991).
[30] L. K. Fenton, J. L. Bandfield, and A. W. Wartd, J. Geophys. Res. **108**, 5129 (2003).
[31] H. Tsoar and K. Pye, Sedimentology **34**, 139 (1987).
[32] J. A. Jiménez and O. A. Madsen, J. Waterway, Port, Coastal, Ocean Eng. **130**, 220 (2003).
[33] P. Claudin and B. Andreotti, Earth Planet. Sci. Lett. **252**, 30 (2006).
[34] S. G. Fryberger and G. Dean, in *A Study of Global Sand Seas*, edited by E. D. McKee (United States Geological Survey, Washington, D.C., 1979), Professional Paper 1052, p. 137.
[35] R. S. Anderson and P. K. Haff, Acta Mech. **1**, 21 (1991).
[36] G. R. Butterfield, in *Turbulence: Perspectives on Flow and Sediment Transport*, edited by N. J. Clifford, J. R. French, and J. Hardisty (Wiley, New York, 1993), Chap. 13, p. 305.
[37] I. K. McEwan and B. B. Willetts, Acta Mech. **1**, 53 (1991).
[38] M. C. Bourke, M. Balme, and J. Zimbelman, Proc. Lunar Planet. Sci. Conf. **35**, 1453 (2004).
[39] E. J. R. Parteli, O. Durán, and H. J. Herrmann, Phys. Rev. E **75**, 011301 (2007).
[40] J. L. Sutton, C. B. Leovy, and J. E. Tillman, J. Atmos. Sci. **35**, 2346 (1978).
[41] R. S. Anderson and P. K. Haff, Science **241**, 820 (1988).
[42] B. Andreotti, J. Fluid Mech. **510**, 47 (2004).
[43] K. Kroy, S. Fischer, and B. Obermayer, J. Phys.: Condens. Matter **17**, S1299 (2005).
[44] N. S. Embabi and M. M. Ashour, J. Arid Environ. **25**, 49 (1993).
[45] M. C. Bourke, K. S. Edgett, and B. A. Cantor, Geomorphology (to be published).
[46] P. Hersen, S. Douady, and B. Andreotti, Phys. Rev. Lett. **89**, 264301 (2002).
[47] P. Lee and P. C. Thomas, J. Geophys. Res. **100**, 5381 (1995).
[48] E. J. R. Parteli, O. Durán, H. Tsoar, V. Schwämmle, and H. J. Herrmann (unpublished).
[49] M. C. Bourke, Proc. Lunar Planet. Sci. Conf. **37**, 2432 (2006).
[50] R. E. Arvidson, E. A. Guinness, and S. Lee, Nature (London) **278**, 533 (1979).
[51] W. Fernández, Earth, Moon, Planets **77**, 19 (1998).
[52] M. C. Malin, M. H. Carr, G. E. Danielson, M. E. Davies, W. K. Hartmann, A. P. Ingersoll, P. B. James, H. Masursky, A. S. McEwen, L. A. Soderblom, P. Thomas, J. Veverka, M. A. Caplinger, M. A. Ravine, T. A. Soulanille, and J. L. Warren, Science **279**, 1681 (1998).
[53] P. C. Thomas, J. Geophys. Res. **87**, 9999 (1982).
[54] P. C. Thomas, M. C. Malin, M. H. Carr, G. E. Danielson, M. E. Davies, W. K. Hartmann, A. P. Ingersoll, P. B. James, A. S.

Mcewen, L. A. Soderblom, and J. Veverka, Nature (London) **397**, 592 (1999).
[55] W. Sheehan, *The Planet Mars: A History of Observation and Discovery* (The University of Arizona Press, Tucson, 1996).
[56] I. Livingstone, Sedimentology **36**, 1017 (1989).
[57] H. Tsoar, Sedimentology **30**, 567 (1983).
[58] H. Tsoar, Physica A **357**, 50 (2005).
[59] V. Schatz, H. Tsoar, K. S. Edgett, E. J. R. Parteli, and H. J. Herrmann, J. Geophys. Res. **111**, E04006 (2006).
[60] O. Durán, Ph.D. thesis, Universität Stuttgart, 2007 (unpublished).
[61] E. J. R. Parteli, Ph.D. thesis, Universität Stuttgart, 2007 (unpublished).
[62] D. J. Jerolmack, D. Mohrig, J. P. Grotzinger, D. A. Fike, and W. A. Watters, J. Geophys. Res. **111**, E12S02 (2006).
[63] M. P. Almeida, J. S. Andrade, Jr., and H. J. Herrmann, Phys. Rev. Lett. **96**, 018001 (2006).